Journal of the Australian Ceramic Society (2021) 57:1379–1388
https://doi.org/10.1007/s41779-021-00634-w

RESEARCH

ZnO/Al_2O_3 layered structures deposited by RF magnetron sputtering on glass: growth characteristics, optical properties, and microstructural analysis

Ebru Şenadım Tüzemen[1,2] · Ali Özer[3,4] · İlkay Demir[2,5] · İsmail Altuntaş[2,5] · Mehmet Şimşir[3,4]

Received: 12 December 2020 / Revised: 20 June 2021 / Accepted: 29 June 2021 / Published online: 12 August 2021

Abstract

In this study, Al_2O_3 thin films of different thicknesses (50 nm, 100 nm, 150 nm, 200 nm, and 250 nm) were, first, grown using RF magnetron sputtering technique on glass substrate at 30 °C temperature, with 120 W power value. Then 250 nm ZnO was grown on these thin films. Microstructural analyses of the thin films were made by scanning electron microscope (SEM). It was observed that the particle size changed with increasing thickness of Al_2O_3 thin films. ZnO layer was grown onto alumina grown tubes with an approximate thickness of 250 nm. The grain morphology of ZnO was similar to alumina, about 25–30 nm grain size. Energy-dispersive X-ray analysis (EDX) detector was used to determine the chemical composition of the samples. These results have indicated that ZnO thin films are successfully formed on alumina tubes. Crystal structure analyses of all samples were examined using the X-ray diffraction (XRD) technique. In addition, the optical properties of the samples were examined with ultraviolet-visible-near infrared spectrometer (UV-VIS-NIR). This work provides valuable references for the application of Al_2O_3 as insulating buffer layers.

Keywords Al_2O_3 · ZnO · Magnetron sputtering · SEM · XRD · Optical properties

Introduction

In the last few decades, transparent conductive oxides, such as ZnO, ITO, and CdO, have attracted great attention among researchers due to their unique properties which are reflecting the light in the visible region and transparent and conductive nature. Because of these, they are preferred in many scientific researches and industrial applications. In addition, these oxide materials are the most preferred materials among metal oxide semiconductors especially since they have reflection property in the visible region.

ZnO is a semiconductor with a hexagonal wurtzite crystal structure, and it is an n-type semiconductor material with high conductivity, high transmittance, wide band gap of 3.3 eV, and 60 meV exciton binding energy at room temperature [1]. Due to these properties, it is one of the most popular materials among transparent conductive oxide materials. ZnO semiconductor compound has a high breakdown voltage and high melting temperature (1975 °C). For these reasons, nano-sized ZnO materials can be used in temperature control circuits operating at high power and frequency, and in the composition of sunscreen creams in the cosmetics industry due to their transparency. So, it has also become a candidate material, which will be used in solar cells, gas sensors, different types of transducers, luminescent materials, transparent conductors, heat mirrors, and semiconductor heterogeneous intersections [2, 3].

Alumina started to be used commercially for the first time in 1907 with a patent taken on a high alumina ceramic production. It is widespread commercial production, and use took

✉ Ebru Şenadım Tüzemen
esenadim@cumhuriyet.edu.tr

[1] Nanophotonics Research and Application Center, Sivas Cumhuriyet University, 58140 Sivas, Turkey

[2] Department of Physics, Faculty of Science, Sivas Cumhuriyet University, 58140 Sivas, Turkey

[3] Department of Metallurgical and Materials Engineering, Sivas Cumhuriyet University, 58140 Sivas, Turkey

[4] Advanced Technology R & D Center, Sivas Cumhuriyet University, 58140 Sivas, Turkey

[5] Department of Nanotechnology Engineering, Sivas Cumhuriyet University, 58140 Sivas, Turkey

place in the early 1930s. Pure alumina is available in different forms at low temperatures. However, depending on the crystal size of alumina, the atmosphere of the medium, and time, its all forms transform into α-Al_2O_3 at temperatures between 750 and 1200 °C. This transformation accelerates much more after at above 1600 °C which is an irreversible process for α-phase alumina. On the other hand, alumina provides good hardness, high refractoriness, and chemical stability; however, its strength and fracture toughness are very low. Strength drops significantly at elevated temperatures over 700 °C as well as its thermal shock resistance. Alumina, which has properties to be used as a catalyst and catalytic support material, is used in a wide range of fields such as optical applications, insulation material, making abrasive and cutting tools, ceramic and refractory materials, dental prostheses, bone and dental implants, integrated circuit packages, and wastewater treatment. [4–10].

ZnO is very suitable for forming bilayer nanostructures. There are some studies carried out on the growth of ZnO films on alumina in literature. Zaka et al. [11] have investigated Al_2O_3/ZnO bilayer and Al_2O_3/Al_2O_3-ZnO mixed oxide/ZnO trilayer samples which were prepared by atomic layer deposition (ALD) technique. They focused on how to develop the optical properties of these sample systems and how it is affected by the stacking of Al_2O_3 and ZnO layers. They have analyzed the transmission, refractive index, extinction coefficient, and reflection spectra of the films. Viter et al. [12] have studied optical and structural properties of ultrathin Al_2O_3/ZnO nanolaminates deposited by ALD. Cui et al. [13] have fabricated fully transparent high-performance thin-film transistors (TFTs) with a bottom-gate structure by ALD at low temperature. The TFTs with the ZnO/15-cycle Al_2O_3/ZnO structure exhibited superior performance with a low threshold voltage (VTH) of 0.9 V, a high saturation mobility (μ_{sat}) of 145 cm^2V^{-1} s^{-1}, a steep subthreshold swing (SS) of 162 mV/decade, and a high I_{on}/I_{off} ratio of 3.15 10^8. Hadi et al. [14] have worked on the effects of the Al_2O_3/ZnO ratio on the optical and electrical properties of aluminum-doped ZnO (AZO) layers deposited by atomic layer deposition. They reported complex refractive indices for AZO layers with different numbers of aluminum atomic cycles (ZnO/Al_2O_3 =1:0, 39:1, 19:1, and 9:1). Kim et al. [15] have studied ZnO film on Al_2O_3/Si by ALD at 150 °C process temperature. ZnO/Al_2O_3/Si and ZnO/Si structures annealed at high temperature (⩾800 °C) were investigated to see the effect of Al_2O_3 buffer layer. Romo-Garcia et al. [16] have studied on the ZnO and Al_2O_3 nanolaminates that they have grown using a homemade ALD technique. They have synthesized three samples with a multi-film structure that was formed by four Al_2O_3/ZnO bilayers of 20 nm. The thickness of the Al_2O_3 was varied at 1%, 3%, and 5% of the total bilayer width for each sample. Lopez et al. [17] have studied the ultrathin multilayer films of Al_2O_3-ZnO bilayers grown by the ALD technique onto (100) Si substrates. A set of 10 samples based on bilayers with various 2:X thickness ratios were prepared, where X refers to the ZnO layer thickness. X is proportional to the number of cycles (N) of the ZnO precursor, varying from 1 to 100. Al_2O_3/ZnO nanolaminates (NLs) with various ZnO sublayer thicknesses were grown using atomic layer deposition by Li et al. [18]. Wang [19] has deposited the ZnO/Al (AZO) films on glass substrates with Al_2O_3 buffer layers by RF magnetron sputtering.

In this study, Al_2O_3/ZnO structures were deposited on glass substrates using the RF magnetron sputtering method. We focused on how the optical and structural properties were affected by different Al_2O_3 film thicknesses as a buffer layer in Al_2O_3-ZnO multilayers. The structural formation of Al_2O_3 sublayers was characterized using XRD, and amorphous phase formation of the ZnO sublayers exhibited an oriented polycrystalline structure. We observed hexagonal structure for the film with preferred orientation of (002) plane.

Experimental details

In this study, we investigated Al_2O_3/ZnO film formation on a glass substrate to determine structural and optical properties. Glass substrates were firstly cleaned with deionized water, isopropyl alcohol, and acetone and then dried with blowing air. Al_2O_3 (purity of 99.99%) and ZnO purity of 99.9%) targets were purchased from Plasmaterials Co. Inc. with a diameter and thickness of 2 in. × 0.125 in. Al_2O_3 and ZnO targets were used in magnetron sputtering, and a non-reactive sputtering process was applied. We denoted two groups of samples: the first group is the formation of monolayer Al_2O_3 thin film on glass substrate with a thickness of 50, 100, 150, 200, 250 nm, and 250 nm of ZnO thin film and labeled as A50, A100, A150, A200, A250, and Z250 nm, respectively. All parameters of film growth, base pressure (Torr), work pressure (mTorr), rotate (rpm), power (W), and thickness (nm) are summarized in Table 1. The second group is depositing 250 nm of ZnO film on the Al_2O_3 films in the first group and denoted as A50-Z250, A100-Z250, A150-Z250, A200-Z250, and A250-Z250. The schematic representations of monolayer Al_2O_3 and bilayer Al_2O_3/ZnO thin film samples are given in Fig. 1.

Before the film depositions, glass substrates were heated to 30 °C, and the distance between the target and substrate was adjusted to 6.5 cm. After the glass substrates were placed on the holders in chamber, then the lid was closed and the system was pumped to lower the base pressure down to 1.8 $x10^{-6}$ torr (see Table 1). When we reach the base pressure, argon gas was introduced into the film growth medium. The power value from the RF power supply unit was set to 120 W for Al_2O_3 and 60 W for ZnO, and a pre-splash was made from the target surface for 15 min. As illustrated in Fig. 1, the Al_2O_3

Table 1 The applied parameters of RF sputtering system for the monolayer Al_2O_3 and ZnO thin films are base pressure (Torr), work pressure (mTorr), rotate (rpm), power (W), and thickness (nm).

Sample name	Base pressure (Torr)	Work pressure (mTorr)	Rotate (rpm)	Power (W)	Thickness (nm)
A50	1.85×10^{-6}	13	5	120	50
A100	1.42×10^{-6}	13	5	120	100
A150	1.73×10^{-6}	13	5	120	150
A200	1.86×10^{-6}	13	5	120	200
A250	1.82×10^{-6}	13	5	120	250
Z250	1.84×10^{-6}	13	5	60	250

monolayer was deposited on glass substrates by increasing thickness from 50 to 250 nm. Then, 250 nm ZnO film was deposited on each thickness of the alumina layer to produce bilayer coatings. A total of ten films were produced from Al_2O_3.

After the alumina coating procedure, ZnO coating was applied onto the glass substrates which were alumina coated at 7 mTorr onto 150 nm alumina to evaluate the effect of ZnO on alumina-coated glass substrates. This choice was attributed to the tube structure of alumina that is crystallographically similar with ZnO as being both hexagonal.

Characterization of the samples was performed by the techniques as follows: crystal structures of the samples were examined by X-ray diffractometer (PANalytical Empyrean XRD model). The surface morphology of the samples was determined by scanning electron microscopy (TESCAN® MIRA3 XMU (Brno, Czechia) at an accelerating voltage of 10 kV). Optical characterization of the samples was carried out using a double-beam UV-Vis-NIR spectrophotometer (Cary 5000). Optical transmission of samples was taken in the wavelength range of 350–800 nm using a solid sample holder accessory. NANOVAK NVTS-400-2TH2SP Thermal & Sputter Combined System was used to produce Al_2O_3 and ZnO films.

Results and discussion

X-ray diffraction (XRD)

XRD patterns of Al_2O_3 thin films of five different thicknesses deposited on glass substrates are given in Fig. 2a. As it is seen from this figure, the A50 and A100 samples exhibited amorphous structures. Diffraction pattern peaks were observed only for the A150 sample (Table 2) that may be concluded as the thickest tube formation of polycrystalline alumina with differentiated planar distances. However, it is observed that these peaks belonging to A200 and A250 began to disappear. This may be attributed to the sudden closure of alumina tubes and seed formation on the surface to produce amorphous-like or nanoclusters.

These disappeared peaks can be the result of an increase in FWHM values as seen in Table 2. For the bilayer structures, the single diffraction peak of ZnO film was observed that belongs to the (002) plane [18]. As seen in Fig. 2b, the peak of ZnO (002) corresponding to the hexagonal structure was obtained in all samples. The A50-Z250-layered structure has the highest intensity. In the A100-Z250, the existence of peaks decreased and then started to increase again which in turn may be due to the growth of alumina tubes.

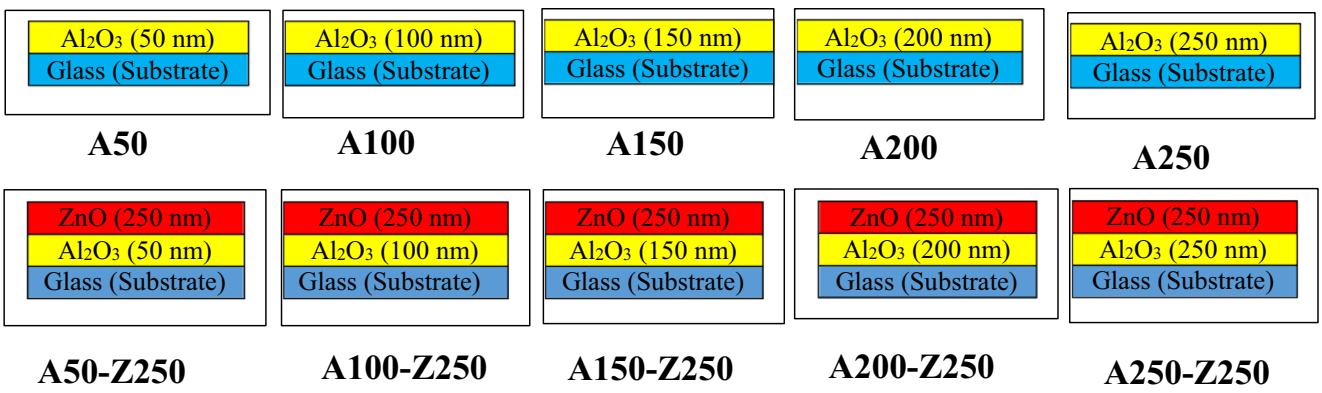

Fig. 1 Schematic representation of the samples deposited on glass substrate by RFMS

Table 2 Values of Bragg's 2θ angle, d-spacing, assignments, and crystallite size of the samples.

	2θ (deg)	d-spacing (Å)	Assignments	Crystallite size (Å)
A50	Amorphous			
A100	Amorphous			
A150	26.7726	3.32720	(012) [20]	1087
	28.6024	3.11838	(213) [21, 22]	1217
	45.4041	1.99591	(400) [23]	717
A200	Amorphous-like or nanoclusters			
A250	Amorphous-like or nanoclusters			
A50-Z250	34.1394	2.62422	(002)	284
A100-Z250	34.1149	2.62604	(002)	255
A150-Z250	34.0677	2.62958	(002)	238
A200-Z250	34.1418	2.62404	(002)	286
A250-Z250	34.0841	2.62835	(002)	265

Morphological properties

The SEM images of the alumina thin film surfaces (A50, A100, A150, A200, and A250) and the surface roughness of the samples are presented in Fig. 3 a, b, c, d, e, and f, respectively. The seeds of alumina coatings were obtained from RFMS coating at 13 mTorr in Fig. 3(a), and the average size of the seeds was found to be 26 nm ± 3 nm. Applying the coating technique, a flat layered-like structure, on which only seeds are seen on the substrate and there is no lateral growth, was formed. The inset picture is seen as the flat layer structure of alumina grown surface about 60 nm ±13 nm thicknesses which is also evident as flattened in Fig. 3(f) for (a) line that has a smoother surface roughness profile. The longitudinal growth of alumina tube or sword-like needles began to form in Fig. 3(b) at the same vacuum condition. The surface is not fairly uniform and has gaps between the needle-like formations. The needles are coarsened and agglomerated due to the attraction of alumina seeds at lower vacuum as illustrated by blue arrows on Fig. 3(b). Since the amorphous glass has an oxide-hydroxide-rich top layer that may attract only the oxide species and has a lower amount of Al element that may be the preferable sites for alumina deposition, this may favor the growth of alumina tube-like structures which is about 100 nm ±21 nm (inset of Fig. 3(b)). The agglomerated and abnormally growth seeds of alumina have a deteriorating effect on the roughness profile as seen in Fig. 3(f) as (b) line. There may be some coarsened alumina regions to affect the

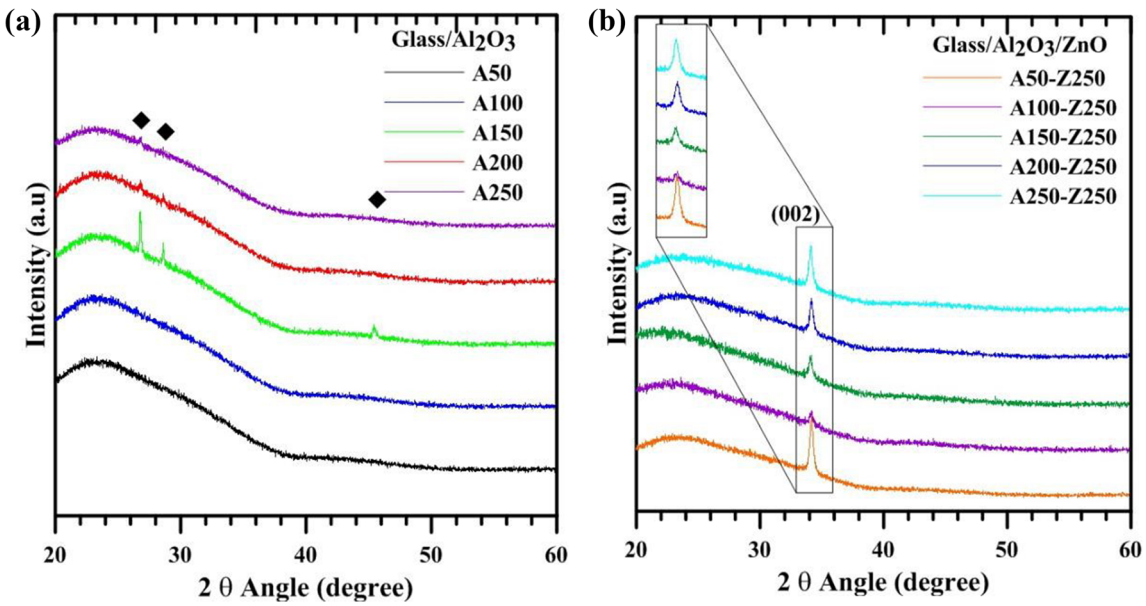

Fig. 2 X-ray diffraction patterns of **a** Al_2O_3 thin films with different thicknesses denoted by A50, A100, A150, A200, and A250 and **b** Al_2O_3/ZnO structures obtained by growing ZnO thin films with 250 nm onto Al_2O_3 thin films with different thicknesses denoted by A50-Z50, A100-Z100, A150-Z150, A200-Z200, and A250-Z250, respectively

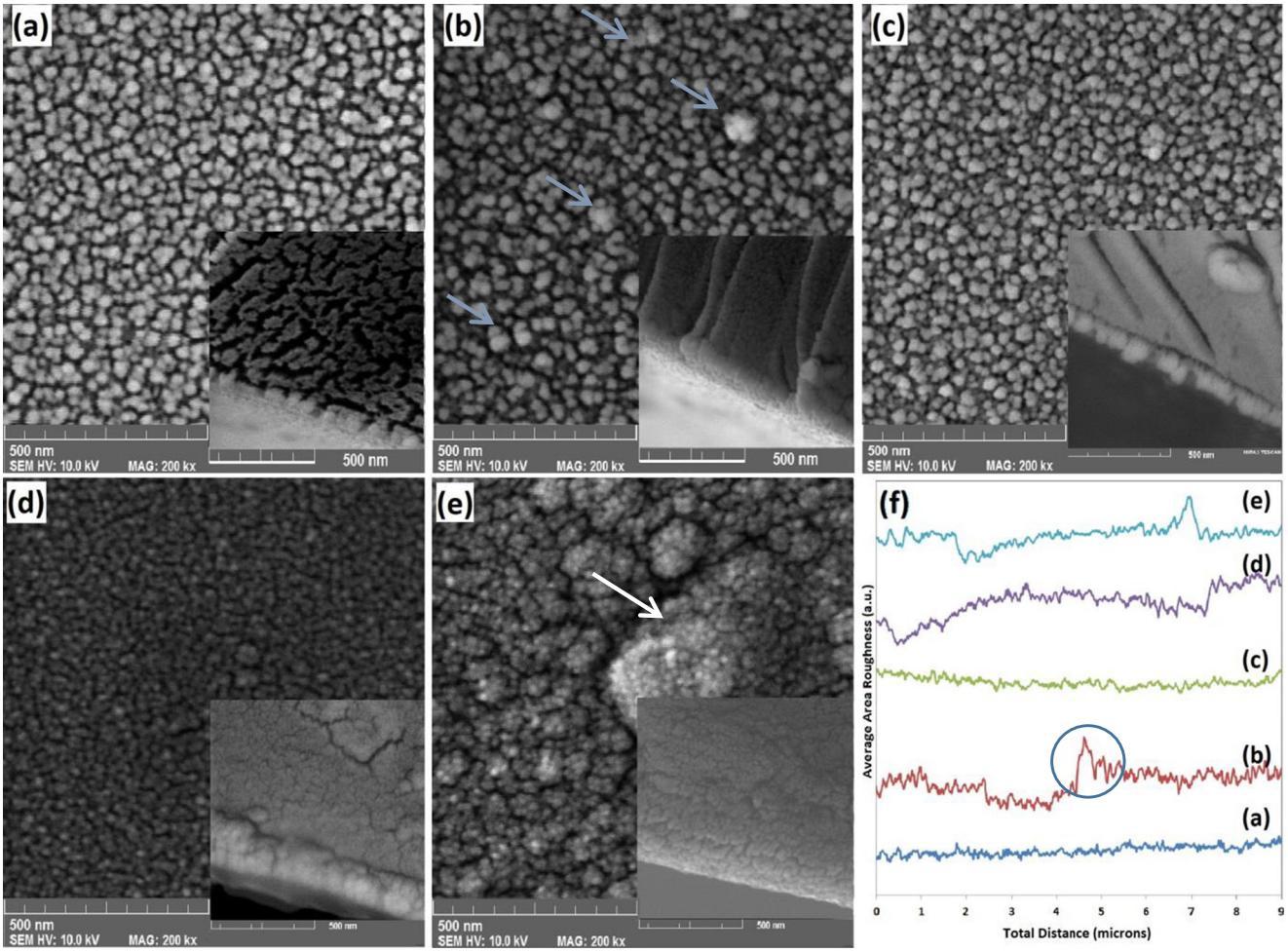

Fig. 3 The surface SEM images of the alumina thin film samples: (a) A50, (b) A100, (c) A150, (d)A200, (e) A250, and (f) surface roughness of the samples.

profile as indicated with the blue circle. There may be even smaller or thinner agglomerates which also deform the regular tube formation on the surface.

Figure 3(c) shows the RFMS coating of A150 sample. The surface shows the fulfilled layers with a fairly smooth surface formation, and the seeds are grown together without agglomeration. There are no large gaps as in Fig. 3(b), and the seed dimensions are very close to each other as to be 27 nm ±3 nm which is very similar to Fig. 3(a) but produces a longitudinal tube of the structure of alumina about 150 nm. The growth of alumina tubes is fed by the closer neighbors that grow afterward and continue to increase the thickness of the tubes away from the substrate. In the inset of Fig. 3(c), it is seen that alumina tubes about 150 nm in length exhibit the smooth surface formation that is confirmed by the roughness line of Fig. 3(f) are grown.

Figure 3(d) shows the alumina coating onto the glass substrate at a constant vacuum by increasing the deposition rate, even if the fine seeds are produced. It is seen that these seeds grow individually and without any agglomeration. The inset shows that the deposition rate is very high and no lateral growth of alumina tubes was seen. This may be attributed to the low vacuum condition, and this condition can be thought of as the coating limit as 200 nm ±17 nm for fine seeds. Hence this condition may cause an increase in the growth rate of the deposited layer and like a change in its growth from lateral tube structure to the layer deposition.

The surface roughness measurements in Fig. 3(f) for (d) line show the deteriorated deposition structure that increases the thickness abnormally. In Fig. 3(f) for (d) line, the fast deposition rate produces a hump with valleys on both sides without any agglomeration of seeds. The average seed diameter was found to be 22 nm ± 2 nm which indicates the individual seed growth.

Figure 3(e) stands for the coating of alumina as the highest deposition rate and thickness produces agglomerated seeds and thus the average diameters of seeds were obtained around 62 nm ± 38 nm as indicated by a white arrow. As seen, the standard deviation is very high, and some abnormally and agglomerated seeds are evident. The very fine seeds on that abnormal grown seeds have an average diameter of 27 nm. This high rate shows itself on Fig. 3(f) for (e) line, by

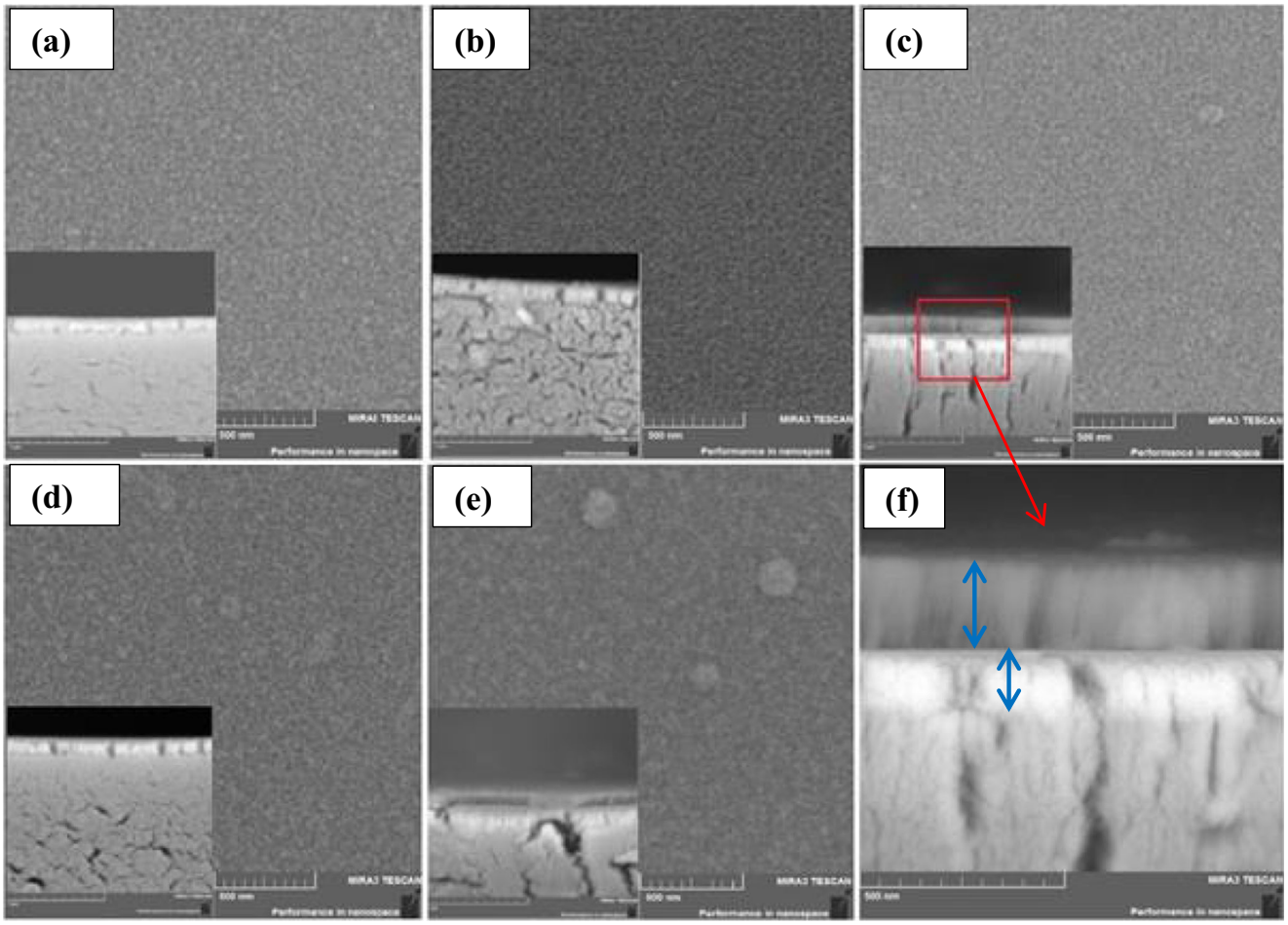

Fig. 4 SEM photos of 250 nm ZnO coating onto corresponding alumina-coated glass surfaces.

deformed surface roughness graph. Some hills and valleys are formed during the coating by the high rate which also resulted in the abnormal agglomeration of seed clusters, while valleys remain unfilled possibly with very fine seeds. As seen from SEM images, the alumina was grown on a glass substrate by applying the same vacuum conditions. The corresponding surface roughness graphs were also indicated in Fig. 3(f). From this point on, the alumina coatings were optimized experimentally and found to be grown on glass up to 150 nm for 13 mTorr which has sword-like or tube structure.

SEM images of ZnO coatings onto alumina-coated glass are seen in Fig. 4(a–f). Figure 4(a) shows the 250 nm ZnO coating at 13 mTorr vacuum condition onto 50 nm alumina-coated glass substrate. The coating in (a) seems to have an embedded alumina layer, while ZnO is deposited on it. ZnO has a layer-plate-like structure. The ZnO layer is very thin and the adaptation onto the surface is poor. The ZnO coating has seeds on the surface which are the nuclei sites for upcoming ZnO sputter. The alumina coating is still visible as a smooth surface, but some seeds of ZnO are also evident.

Figure 4(b) is the SEM coating image of ZnO onto 100 nm alumina-coated glass. The alumina on glass, after ZnO coating, is not visible due to increased ZnO coating layer up to 100 nm. The alumina penetration into glass can be concluded by the effect of ZnO on the surface crystallization of alumina on glass and the low layer thickness of alumina that may diffuse into the glass substrate as well. ZnO layer was grown in a tubular structure which may be an extension of alumina

Table 3 Thickness measurements of the samples from RFMS and SEM

	A50	A100	A150	A200	A250	A50-Z250	A100-Z250	A150-Z250	A200-Z250	A250-Z250
RFMS (nm)	50	100	150	200	250	50-250	100-250	150-250	200-250	250-250
SEM (nm)	64±7	93±7	132±15	190±13	242±11	64±7-120±10	93±7-253±8	132±15-232±8	190±13-252±4	242±11-197±4

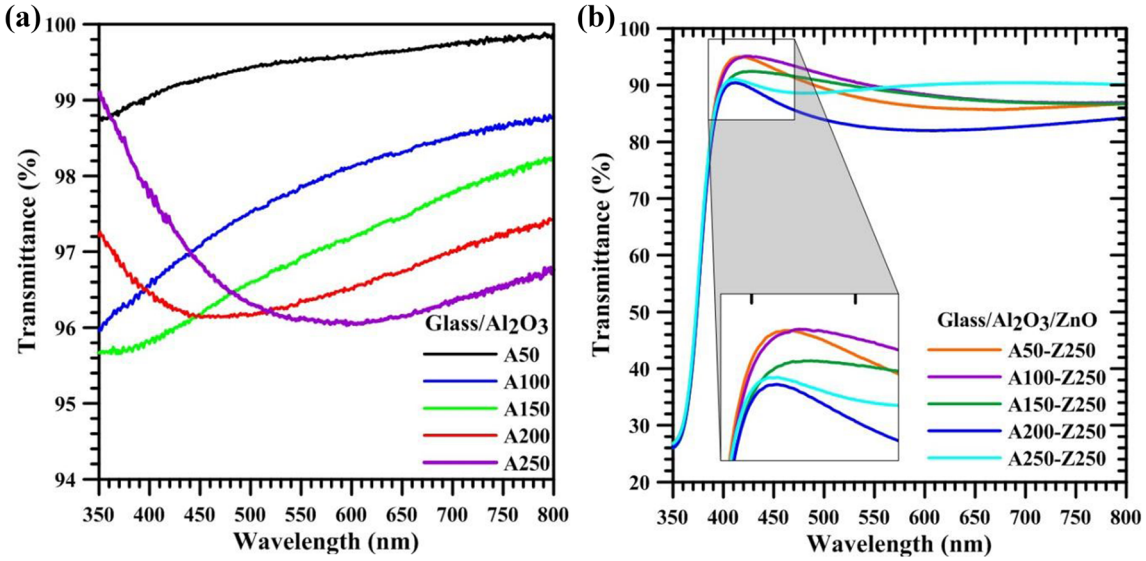

Fig. 5 Transmission spectra of **a** Al_2O_3 and **b** Al_2O_3/ZnO samples

undercoating. Since the alumina has a preferred tubular structure on the glass by hydroxyl similarity on the surface due to the hexagonal structure of ZnO, the ZnO layer may also prefer an orientation in the long axis of crystal structure. Figure 4(c) shows the SEM photo of 250 nm ZnO upper layer coating onto 150 nm alumina-coated glass substrate. Figure 4(f) is the high magnification image of the inset in Fig. 4(c) as indicated by red square and arrow. The surface in Fig. 4(c) has fully seeded, and a low level of agglomeration is seen due to the high thickness of ZnO which also preferred to be grown as a tubular structure. The tubular structure may also be an indicator of the c axis growth of hexagonal ZnO layer on alumina with 150 nm thickness. The thickness measurement was performed in the post-processing program of SEM (Mira TC®) as illustrated in Fig. 4(f) by blue double-sided arrows. The lower layer is seen about 150 nm of alumina on the glass, while the upper arrow shows 250 nm of ZnO coating. The alumina coating seems to be penetrated into glass but shows a brighter scatter due to the higher atomic density of alumina than glass. ZnO tubular structure has a long axis columnar growth of the hexagonal crystal. Since the alumina is also in a possibly hexagonal structure, there may be a lattice match that can favor the tubular growth of ZnO. After this point in Fig. 4(d), the ZnO seed agglomeration increases by increased underlayer coating of alumina which may have produced some defects such as oxygen vacancies. This phenomenon can be understood by the possibility of ZnO to fill the alumina interseed gaps and prevents the increase of ZnO thickness increment on alumina. The alumina itself may also penetrate glass substrate, and the remaining alumina also favors the tubular growth of ZnO to some extent. Figure 4(e) shows the highest thickness values for both Al_2O_3 and ZnO, as being 250 nm for each. Al_2O_3 coating is still seen tubular, while ZnO growth is seen as limited. This low thickness of ZnO may be attributed to the increasing resistance of alumina coating onto the glass. The increased resistance may scatter electrons and does not give them much chance to hold on the surface. As indicated in Fig. 3(e), the deteriorated surface features can be another reason not to increase in thickness for ZnO, since ZnO must fill the gaps first, then real thickness may be seen that may be time-consuming, and 250 nm ZnO coating thickness was calculated by layer thickness measuring sensors. As very well known, these sensors start measuring the layer right after the shutter opened with regard to deposition onto the layer while the sensors themselves were also coated up to 250 nm. Thickness values adjusted from the RFMS device and measured from SEM are shown in Table 3. As can be seen from Table 3, the thicknesses were measured very close for each layer.

Optical properties

The transmittance (T%) of the films was measured at room temperature with a spectrophotometer. The graph of transmittance versus wavelength of Al_2O_3 films obtained in different thicknesses is given in Fig. 5a. From the graph of the optical

Table 4 Optical energy band gap with Tauc and band tail Urbach energy of samples

	A50-Z250	A100-Z250	A150-Z250	A200-Z250	A250-Z250
Tauc (eV)	3.27	3.27	3.28	3.28	3.28
Band tail (meV)	91.95	95.85	103.35	103.48	99.8

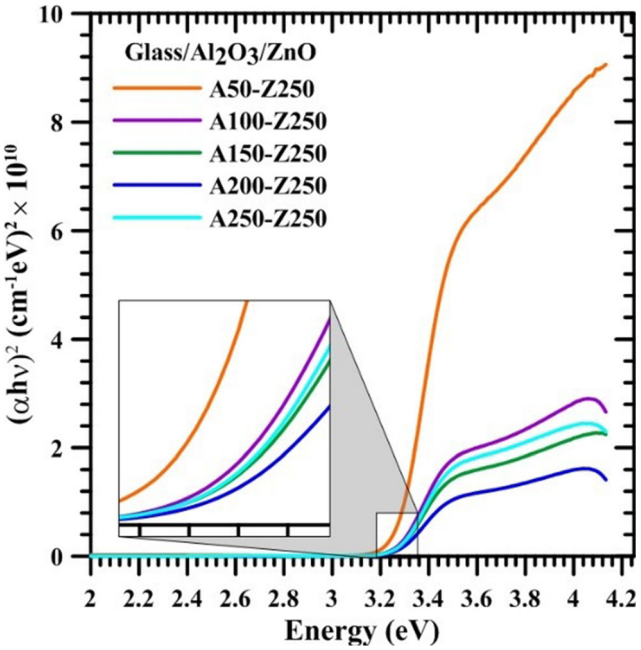

Fig. 6 Bandgap from the plot of $(\alpha h\nu)^2$ as a function of photon energy ($h\nu$).

transmittance versus wavelength of Al_2O_3 films obtained in different thicknesses shown in Fig. 5a, it was observed that the transmittance decreases in the visible region as the thickness increases due to the bulk characteristics of alumina after thicker coatings. In Fig. 5b, the change of the transmittance of the Glass/Al_2O_3/ZnO structures according to the wavelength is seen. As can be seen from the graph, firstly the transmittance of the A50-Z250 and A100-Z250 samples has increased which can be attributed to the decrease in relative surface roughness and formation of a defect-free surface. It has decreased after coating A150-Z250 which in turn due to the thickness increment and preferred orientation of alumina tubes as well as ZnO coating.

Al_2O_3 is widely used as an insulator material [24]. Therefore, it can be used as a buffer layer to increase the crystal and optical quality of materials. In this study, it is clearly seen that Al_2O_3 material used as a buffer layer has kept its optical property and crystal quality. As seen in Fig. 5b, it is seen that the transmittance of ZnO changes as the thickness of the buffer layer Al_2O_3 changes. For Fig. 5a, the transmittance of A50 layer on glass increases up to 99.8% due to a decrease in surface roughness which decreases the surface defects to a high extent. By the thickness of alumina coating increasing up to 100 nm as for A100 code on glass, the transmittance increases from 96 to 98.6%. That can be correlated with the seed growth and irregular grain formation by coating. By increasing thickness from A150 to A250, the relative transmittance decreases down to 96.6% by shifting to higher wavelengths as 550–650 nm which can be concluded as greenish light absorption.

In Fig. 5b, ZnO coating thickness onto Al_2O_3 on glass was evaluated. The A50-Z250 coating shifts the absorption wavelength to 410–450 nm but remains higher in intensity as 96%. By A100-Z250 coating, transmittance remains at 96% which reaches a plateau even at a higher wavelength due to surface roughness decrease on the surface that produces a defect-free surface by regular grain formation. By increasing Al_2O_3 thickness as well as Z250 coating coded as A150-Z250, higher ones decreased the intensity down to 90% which forms a blueish color on the surface due to wavelength stabilization by a sharper decrease of wavelength intensity.

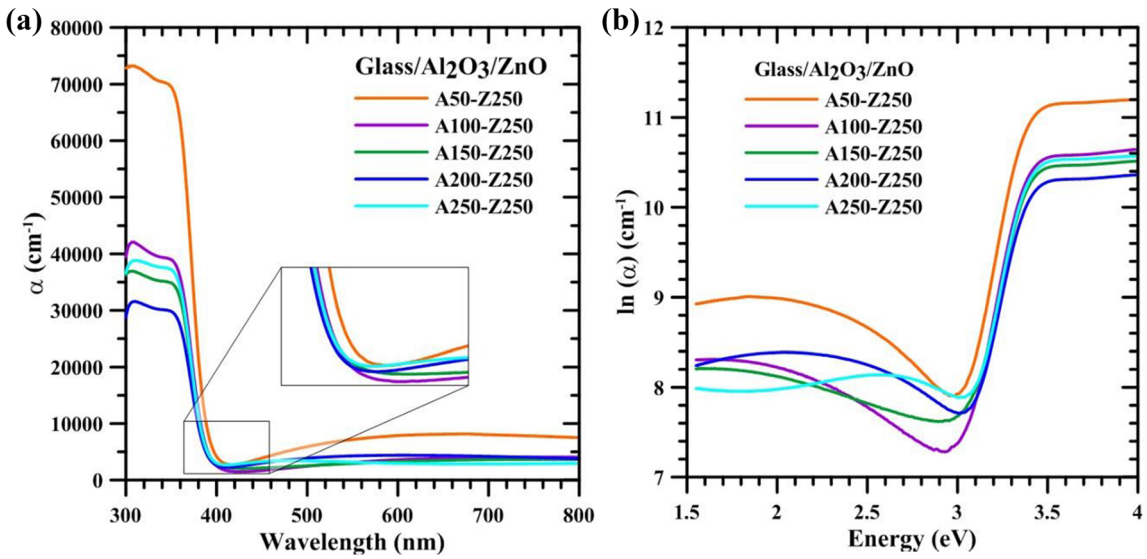

Fig. 7 **a** Absorption coefficient (α) and **b** ln (α) curves versus wavelength and photon energy (hv) of A50-Z50, A100-Zn100, A150-Z150, A200-Z200, and A250-Z250 samples, respectively.

In this study, absorption data are converted into the absorption coefficient by well-known Beer-Lambert laws as given below:

$$\alpha = \frac{1}{d}\ln(T)$$

where T is the transmittance of the thin film and d is the thickness of the film. Energy band gaps have been found by Tauc method [25, 26]. Tauc equation:

$$(\alpha h\nu) = A\left(h\nu - E_g\right)^n$$

is given. Here, $h\nu$ refers to the photon energy, α to the absorption coefficient, A a constant, and E_g energy band gap. In this equation, it takes n =1/2 for the direct band gap and n =2 for the indirect band gap. Since the ZnO film has a direct energy band gap, n = 1/2 was taken. In this equation, α depends on the film thickness for thin films [27, 28].

The graph of calculating the energy band gap for glass/Al_2O_3/ZnO is given in Fig. 6. For this, firstly the graph of $(\alpha h\nu)^2$ with respect to energy has been drawn, and the place where the slope of this graph intersects the energy axis gives the energy band gap of the sample. Energy band gap values found for each sample are given in Table 4. As seen in the table, as the thickness of the multilayer samples increased, the energy band gap raised greater values.

As can be seen in the Fig. 7a, all samples have a sharp absorption edge, and it was observed that absorption started in the UV region in general. The shift of the optical absorption edge of the samples shows that the quality of the films changes with the increase in thickness. It is observed that the absorption edge of the rest of the samples turns to red with the increase in thickness except A250-Z250 sample. In other words, after A200-Z250, the stoichiometry of the samples re-arranged to regular atomic ratios as 2:3 for Al:O and 1:1 for Zn:O (structural defects have decreased).

We can understand this interpretation more clearly by looking at the band tail results (Fig. 7b). In other words, it caused dramatic increases in band tail values of A150-Z250 and A200-Z250 samples (Table 4). As a result, it was seen that these samples had more structural defects than the others.

Conclusions

In summary, monolayer Al_2O_3 and bilayer Al_2O_3/ZnO layers were deposited on the glass substrate by RF magnetron sputtering method, and the structural, morphological, and optical properties of the films were investigated. XRD analysis confirmed the amorphous phase formation for 50, 100, 200, and 250 nm films, except for Al_2O_3 film coated on glass with 150 nm. The highest intensity of glass/Al_2O_3/ZnO structures was obtained in Al_2O_3, which has a thickness of 50 nm. It was observed that the energy band gaps of the films varied between 3.27 and 3.29 eV.

Acknowledgements This study was conducted in Sivas Cumhuriyet University R & D Center (CUTAM), Sivas Cumhuriyet University Nanophotonic Application and Research Center.

Funding This research was supported by Scientific Research Project Fund of Sivas Cumhuriyet University under the project number RGD-32.

References

1. Cho, S., Shim, D.S., Jung, S.H., Oh, E., Lee, B.R., Lee, K.H.: Fabrication of ZnO nanoneedle arrays by direct microwave irradiation. Mater. Lett. **63**, 739–741 (2009)
2. Li, H., Wang, J., Liu, H., Zhang, H., Li, X.: Zinc oxide films prepared by sol–gel method. J. Cryst. Growth. **275**, 943–946 (2005)
3. Bao, D., Gu, H., Kuang, A.: Sol-gel-derived *c*-axis oriented ZnO thin films. Thin Solid Films. **312**, 37–39 (1998)
4. Dey, S.: Synthesis and application of y-alumina nanopowders. National Institute of Technology Department of Chemistry, Rourkela, Thesis (2006)
5. Singh, R.: Synthesis and characterization of hydroxyapatite. Thapar University School of Physics and Materials Science, Patiala, Thesis (2012)
6. Shirai, T., Watanabe, H., Fuji, M., Takahashi, M.: Structural properties and surface characteristics on aluminum oxide powders. Annual report of the advanced ceramics Research Center Nagoya Institute of Technology. **9**, 23–31 (2009)
7. Kumar, R., Prabhakar, V., Saini, J.: Alumina. Int. J. Curr. Eng. Technol. **3**, 1679–1685 (2013)
8. Khazaei, A., Nazari, S., Karimi, G., Ghaderi, E.: Synthesis and characterization of γ-alumina porous nanoparticles from sodium aluminate liquor with two different surfactants. Int. J. Nanosci. Nanotechnol. **12**, 207–214 (2016)
9. Auerkari, P.: Mechanical and physical properties of engineering alumina ceramics. Technical Research Centre of Finland, Finland (1996)
10. Maccauro, G., Rossi Iommetti, P., Raffaelli, L., Manicone, P.F.: Alumina and zirconia ceramic for orthopaedic and dental devices. Biomaterials Applications for Nanomedicine, Italy. 300–309 (2011)
11. Zaka, H., Fouad, S.S., Parditka, B., Bekheet, A.E., Atyia, H.E., Medhat, M., Erdélyi, Z.: Enhancement of dispersion optical parameters of Al2O3/ZnO thin films fabricated by ALD. Sol. Energy. **205**, 79–87 (2020)
12. Viter, R., Baleviciute, I., Abou Chaaya, A., Mikoliunaite, L., Balevicius, Z., Ramanavicius, A., Zalesska, A., Vatamana, V., Smyntyna, V., Gertnere, Z., Erts, D., Miele, P., Bechelanye, M.: Optical properties of ultrathin Al2O3/ZnO nanolaminates. Thin Solid Films. **594**, 96–100 (2015)
13. Cui, G., Han, D., Dong, J., Cong, Y., Zhang, X., Li, H., Yu, W., Zhang, S., Zhang, X., Wang, Y.: Effects of channel structure consisting of ZnO/Al2O3 multilayers on thin-film transistors fabricated by atomic layer deposition. Jpn. J. Appl. Phys. **56**, 04CG03_1-04CG03-4 (2017)
14. Hadi, S.A., Dushaq, G., Nayfeh, A.: Effect of atomic layer deposited Al2O3:ZnO alloys on thin film silicon photovoltaic devices. J. Appl. Phys. **122**, 245103_1-245103_9 (2017)
15. Kim, C.R., Lee, J.Y., Heo, J.H., Shin, C.M., Lee, T.M., Park, J.H., Ryu, H., Chang, J.H., Son, C.S.: Effects of annealing temperature

and Al2O3 buffer layer on ZnO thin films grown by atomic layer deposition. Curr. Appl. Phys. **10**, S298–S301 (2010)
16. Romo-Garcia, F., Higuera-Valenzuela, H.J., Cabrera-German, D., Berman-Mendoza, D., Ramos-Carrazco, A., Tiznado, H., Hirata, G.A., Contreras, O.E., Garcia-Gutierrez, R.: Optoelectronic attenuation behavior of Al2O3/ZnO nanolaminates grown by Atomic Layer Deposition. Thin Solid Films. **669**, 419–424 (2019)
17. Lopez, J., Solorio, E., Borbon-Nunez, H.A., Castillon, F.F., Machorro, R., Nedev, N., Farías, M.H., Tiznado, H.: Refractive index and bandgap variation in Al2O3-ZnO ultrathin multilayers prepared by atomic layer deposition. J. Alloys Compd. **691**, 308–315 (2017)
18. Li, J., Bi, X.: Temperature- and frequency-dependent dielectric behaviors of insulator/semiconductor (Al2O3/ZnO) nanolaminates with various ZnO thicknesses. J. Phys. D. Appl. Phys. **49**, 285301_6 (2016)
19. Wang, X.: Effects of Al2O3 buffer layer on the properties of ZnO: Al thin films deposited on glass by sputtering. Mater. Sci. Forum. **848**, 301–304 (2016)
20. Siva Kumar, V., Kelekanjeri, G., Carter, W.B., Hampikian, J.M.: Deposition of α-alumina via combustion chemical vapor deposition. Thin Solid Films. **515**, 1905–1911 (2006)
21. Toledo, R.R., Santoyo, V.R., Esparza, L.M.A., Larios, A.P., Rosales, M.M.: Study of arsenic (V) removal of water by using agglomerated alumina. Nova Scientia. **11**, 1–25 (2019)
22. Karunakaran, C., Anilkumar, P., Gomathisankar, P.: Photoproduction of iodine with nanoparticulate semiconductors and insulators. Chem. Cent. J. **5**(31), 1–9 (2011)
23. Gheorghies, C., Gheorghies, L., Ciortan, S., Paunoiu, V., Cantaragiu, A. M., Lalau, C. C., Rusu, D. E.: Structural analysis of alümina thin layer prepared by controlled oxidation process. The annals of "Dunărea de Jos" University of Galaţi Fascicle V, Technologies in Machine Building. ISSN: 1221-4566, 319–322 (2009)
24. Lu, H.L., Gu, Y.Z., Zhang, Y., Liu, X.Y., Wang, P.F., Sun, Q.Q., Ding, S.J., Zhang, D.W.: Improved photoelectrical properties of n-ZnO/p-Si heterojunction by inserting an optimized thin Al_2O_3 buffer layer. Opt. Express. **22**, 22184–22189 (2014)
25. Chaaya, A.A., Viter, R., Bechelany, M., Alute, Z., Erts, D., Zalesskaya, A., Kovalevskis, K., Rouessac, V., Smyntyna, V., Miele, P.: Evolution of microstructure and related optical properties of ZnO grown by atomic layer deposition. Beilstein J. Nanotechnol. **4**, 690–698 (2013)
26. Chaaya, A.A., Viter, R., Baleviciute, I., Bechelany, M., Ramanavicius, A., Gertnere, Z., Erts, D., Smyntyna, V., Miele, P.: Tuning optical properties of Al2O3/ZnO nanolaminates synthesized by atomic layer deposition. J. Phys. Chem. C. **118**, 3811–3819 (2014)
27. Saleh, W.R., Saeed, N.M., Twej, W.A., Alwan, M.: Synthesis sol-gel derived highly transparent ZnO thin films for optoelectronic applications. Adv. Mater. Phys. Chem. **2**, 11–16 (2012)
28. Sardela, M.: Practical materials characterization. Springer, New York, ISBN:978-1-4614-9280-1 (2014)